

University of Wisconsin - Madison

MAD/PH/834

UCD-94-23

June 1994

W and Z Polarization Effects in Hadronic Collisions

E. Mirkes^a and J. Ohnemus^b

^a*Physics Department, University of Wisconsin, Madison, WI 53706, USA*

^b*Physics Department, University of California, Davis, CA 95616, USA*

A Monte Carlo study of the polar and azimuthal angular distributions of the lepton pair arising from the decay of a W or Z boson produced at high transverse momentum in hadronic collisions is presented. In the absence of cuts on the final state leptons, the lepton angular distribution in the gauge boson rest frame is determined by the gauge boson polarization. Numerical results for the lepton angular distributions in the Collins-Soper frame with acceptance cuts and energy resolution smearing applied to the leptons are presented. In the presence of cuts, the lepton angular distributions are dominated by kinematic effects rather than polarization effects, however, some polarization effects are still observable on top of the kinematic effects. Polarization effects are highlighted when the experimental distributions are divided by the Monte Carlo distributions obtained using isotropic gauge boson decay.

I. INTRODUCTION

The measurement of the angular distribution of leptons from the decay of a gauge boson $V \rightarrow l_1 l_2$ [$V = W, Z$] produced in hadronic collisions via a Drell-Yan type process $h_1 + h_2 \rightarrow V + X$ provides a detailed test of the production mechanism of the gauge boson. In the absence of cuts on the final state leptons, the lepton angular distribution in the gauge boson rest frame is determined by the gauge boson polarization. At $\mathcal{O}(\alpha_s)$ in perturbative QCD the angular distribution is described by six helicity cross sections, which are functions of the transverse momentum and rapidity of the gauge boson. The lepton angular distribution can be used to analyze the gauge boson polarization and thereby test the underlying production dynamics in much more detail than is possible by rate measurements alone.

The hadronic production of a vector boson V is described in lowest order [$\mathcal{O}(\alpha_s^0)$] by the Drell-Yan quark-antiquark annihilation process $q\bar{q} \rightarrow V$. In the case of W boson production at low transverse momentum p_T , the W bosons are produced fully polarized along the beam direction due to the pure $V - A$ coupling of the charged currents, and the resulting angular distribution of the charged lepton in the W boson rest frame is simply

$$dN/d(\cos \theta) \sim \text{valence quarks} \otimes (1 + \cos \theta)^2 + \text{sea quarks} \otimes (1 + \cos \theta^2). \quad (1)$$

Here θ denotes the angle between the electron (positron) and the proton (antiproton) direction. The measurement of this angular distribution¹ for the W boson by UA1 [1] and UA2 [2] established the $V - A$ coupling and the spin-1 nature of the W boson. For Z boson production at small p_T , the angular distribution can be parametrized as

$$dN/d(\cos \theta) \sim 1 + A_4 \cos \theta + \cos^2 \theta. \quad (2)$$

The coefficient A_4 depends on the vector and axial-vector couplings of the fermions to the Z boson and is thus sensitive to $\sin^2 \theta_W$. Unfortunately, measurements of the $\cos \theta$ distributions

¹ At the CERN $Spp\bar{S}$ collider energies the contribution from sea quark annihilation is negligible.

for gauge bosons produced at low p_T are only sensitive to the trace of the density matrix elements of the vector bosons.

For gauge bosons produced with transverse momentum [balanced by additional gluons or quarks], the event plane spanned by the beam and gauge boson momentum directions provides a convenient reference plane for studying the angular distributions of the decay leptons. The angular distributions are now sensitive to non-diagonal elements of the gauge boson density matrix elements. In leading order QCD [$\mathcal{O}(\alpha_s)$] the angular distribution has the general form [3]

$$\begin{aligned} \sigma \sim & (1 + \cos^2 \theta) + \frac{1}{2} A_0 (1 - 3 \cos^2 \theta) + A_1 \sin 2\theta \cos \phi \\ & + \frac{1}{2} A_2 \sin^2 \theta \cos 2\phi + A_3 \sin \theta \cos \phi + A_4 \cos \theta, \end{aligned} \quad (3)$$

where θ and ϕ denote the polar and azimuthal angle of the decay leptons in the gauge boson rest frame. Leading order (LO) analytical results for the coefficients A_i for the decay of a W or Z boson in the Collins–Soper [3] frame are discussed in Refs. [4–6]. The complete next-to-leading-order (NLO) corrections to the parity conserving coefficients were calculated in Ref. [6] and were found to be fairly small [less than 10%]. This is because the coefficients A_i are ratios of helicity cross sections [see Eq. (26)] and the QCD corrections tend to cancel in these ratios. LO results for the coefficients A_0, A_1 , and A_2 for a virtual photon² γ^* decaying into two leptons are discussed in Ref. [7]. An investigation of the decay lepton spectrum in the laboratory frame can be found in Ref. [8].

In this paper we present a numerical study of the decay lepton angular distribution for W and Z boson production at the Fermilab Tevatron collider [$\sqrt{S} = 1.8$ TeV]. The calculation includes acceptance cuts on the decay leptons. These cuts are necessary to reduce the background from low p_T jets which can fake electrons. They are also necessary due to the finite acceptance of the detector. Uncertainties due to the finite energy resolution of the detector are simulated in the calculation by Gaussian smearing of the lepton four-

²The parity-violating coefficients A_3 and A_4 vanish in this case.

momentum vectors. The energy resolution smearing has a non-negligible effect only on the $\cos\theta$ distribution of the lepton from W decay. We show the transverse momentum $[p_T(V)]$ dependence of the coefficients A_i and study the effect of the acceptance cuts and energy resolution smearing on the ϕ and $\cos\theta$ distributions in the Collins–Soper (CS) frame. The CS frame has the unique advantage that the polar and azimuthal angles θ and ϕ can be reconstructed modulo a sign ambiguity in $\cos\theta$ without information on the longitudinal momentum of the neutrino.

Since the effects of the NLO corrections are small, it is sufficient to use LO matrix elements in our Monte Carlo study. At NLO there are three more angular coefficients in Eq. (3) which receive contributions from the absorptive part of the one-loop amplitudes. A numerical analysis shows that their contribution is small [at the level of 1% at high p_T] [6], thus they will be neglected in this analysis.

The measurements of the lepton distributions arising from the decay of a virtual photon γ^* in nucleon-nucleon scattering presented in Ref. [9] appear to disagree with the QCD improved parton model. Several different nonperturbative effects have recently been discussed in Ref. [10] to explain the discrepancy. It would be interesting to test whether the angular distributions from W and Z boson decay at the Tevatron are in agreement with theoretical predictions.

The remainder of this paper is organized as follows: the formalism for describing the angular distributions is discussed in Sec. II, numerical results are presented in Sec. III, and summary remarks are given in Sec. IV.

II. ANGULAR DISTRIBUTIONS

We consider the angular distribution of the leptons coming from the leptonic decay of gauge bosons produced with non-zero transverse momentum in high energy proton-antiproton collisions. For definiteness we take

$$p(P_1) + \bar{p}(P_2) \rightarrow W^\pm(Q) + X \rightarrow l^\pm(l_1) + \nu_l(l_2) + X, \quad (4)$$

and

$$p(P_1) + \bar{p}(P_2) \rightarrow Z(Q) + X \rightarrow l^+(l_1) + l^-(l_2) + X, \quad (5)$$

where the quantities in parentheses denote the four-momenta of the particles. In leading order QCD [$\mathcal{O}(\alpha_s)$] the parton subprocesses

$$\begin{aligned} q + \bar{q} &\rightarrow V + g, \\ q + g &\rightarrow V + q, \\ g + \bar{q} &\rightarrow V + \bar{q}, \end{aligned} \quad (6)$$

contribute to high p_T gauge boson production.

In the parton model the hadronic cross section is obtained by folding the hard parton level cross section with the respective parton densities:

$$\frac{d\sigma^{h_1 h_2}}{dp_T^2 dy d\Omega^*} = \sum_{a,b} \int dx_1 dx_2 f_a^{h_1}(x_1, \mu_F^2) f_b^{h_2}(x_2, \mu_F^2) \frac{s d\hat{\sigma}_{ab}}{dt du d\Omega^*} (x_1 P_1, x_2 P_2, \alpha_s(\mu_R^2)), \quad (7)$$

where the sum is over $a, b = q, \bar{q}, g$. $f_a^h(x, M^2)$ is the probability density for finding parton a with momentum fraction x in hadron h when it is probed at scale μ_F^2 . The parton level cross section for the processes in Eq. (6) are denoted by $d\hat{\sigma}_{ab}$. Denoting hadron level and parton level quantities by upper and lower case characters, respectively, the hadron and parton level Mandelstam variables are defined by

$$S = (P_1 + P_2)^2, \quad T = (P_1 - Q)^2, \quad U = (P_2 - Q)^2, \quad (8)$$

and

$$\begin{aligned} s &= (p_1 + p_2)^2 = x_1 x_2 S, \\ t &= (p_1 - Q)^2 = x_1(T - Q^2) + Q^2, \\ u &= (p_2 - Q)^2 = x_2(U - Q^2) + Q^2, \end{aligned} \quad (9)$$

where $p_1 = x_1 P_1$ and $p_2 = x_2 P_2$. The rapidity y of the gauge boson in the laboratory frame can be written

$$y = \frac{1}{2} \log \left(\frac{Q^2 - U}{Q^2 - T} \right), \quad (10)$$

and the transverse momentum p_T of the gauge boson is related to the Mandelstam variables via

$$p_T^2 = \frac{(Q^2 - U)(Q^2 - T)}{S} - Q^2 = \frac{ut}{s}. \quad (11)$$

The angles θ and ϕ in $d\Omega^* = d\cos\theta d\phi$ are the polar and azimuthal decay angles of the leptons in the gauge boson rest frame measured with respect to a coordinate system to be described later.

Technically, the lepton-hadron correlations are described by the contraction of the lepton tensor $L_{\mu\nu}$ with the hadron tensor $H^{\mu\nu}$, where $L_{\mu\nu}$ acts as an analyzer of the gauge boson polarization. The angular dependence in Eq. (7) can be extracted by introducing helicity cross sections corresponding to the non-zero combinations of the polarization density matrix elements

$$H_{mm'} = \epsilon_\mu^*(m) H^{\mu\nu} \epsilon_\nu(m'), \quad (12)$$

where $m, m' = +1, 0, -1$ and

$$\begin{aligned} \epsilon_\mu(\pm 1) &= \frac{1}{\sqrt{2}} (0; \pm 1, -i, 0), \\ \epsilon_\mu(0) &= (0; 0, 0, 1), \end{aligned} \quad (13)$$

are the polarization vectors for the gauge boson defined with respect to the chosen gauge boson rest frame. The angular dependence of the differential cross section can be written [see Ref. [6] for details]

$$\begin{aligned} \frac{16\pi}{3} \frac{d\sigma}{dp_T^2 dy d\cos\theta d\phi} &= \frac{d\sigma^{U+L}}{dp_T^2 dy} (1 + \cos^2\theta) + \frac{d\sigma^L}{dp_T^2 dy} (1 - 3\cos^2\theta) \\ &+ \frac{d\sigma^T}{dp_T^2 dy} 2\sin^2\theta \cos 2\phi + \frac{d\sigma^I}{dp_T^2 dy} 2\sqrt{2}\sin 2\theta \cos\phi \\ &+ \frac{d\sigma^A}{dp_T^2 dy} 4\sqrt{2}\sin\theta \cos\phi + \frac{d\sigma^P}{dp_T^2 dy} 2\cos\theta, \end{aligned} \quad (14)$$

where

$$\begin{aligned}
\sigma^{U+L} &\sim H_{00} + H_{++} + H_{--} , \\
\sigma^L &\sim H_{00} , \\
\sigma^T &\sim \frac{1}{2}(H_{+-} + H_{-+}) , \\
\sigma^I &\sim \frac{1}{4}(H_{+0} + H_{0+} - H_{-0} - H_{0-}) , \\
\sigma^P &\sim H_{++} - H_{--} , \\
\sigma^A &\sim \frac{1}{4}(H_{+0} + H_{0+} + H_{-0} + H_{0-}) .
\end{aligned} \tag{15}$$

The unpolarized differential production cross section is denoted by σ^{U+L} whereas $\sigma^{L,T,I,P,A}$ characterize the polarization of the gauge boson, *e.g.*, the cross section for longitudinally polarized gauge bosons is denoted by σ^L , the transverse-longitudinal interference cross section by σ^I , the transverse interference cross section by σ^T , *etc* (all with respect to the z -axis of the chosen lepton pair rest frame; for details see appendix C of Ref. [6]). At NLO there are three more ‘‘T-odd’’ angular coefficients in Eq. (14) for W and Z production. However, their numerical contribution is small [6,11] and we will neglect them in the present analysis. The helicity cross sections σ^α contain the following coupling coefficients:

$$\sigma^{U+L,L,T,I} \sim (v_l^2 + a_l^2)(v_q^2 + a_q^2) , \tag{16}$$

$$\sigma^{P,A} \sim v_l a_l v_q a_q , \tag{17}$$

where $v_q(a_l)$ and $a_q(a_l)$ denote the vector and axial vector coupling of the gauge boson to the quark (lepton).

The hadronic helicity cross sections $\frac{d\sigma^\alpha}{dp_T^2 dy}$ in Eq. (14) are obtained by convoluting the partonic helicity cross sections with the parton densities:

$$\frac{d\sigma^\alpha}{dp_T^2 dy} = \int dx_1 dx_2 f^{h_1}(x_1, \mu_F^2) f^{h_2}(x_2, \mu_F^2) \frac{s d\hat{\sigma}^\alpha}{dt du} . \tag{18}$$

The helicity cross sections $\hat{\sigma}^\alpha$ are dependent on the choice of the z -axis in the rest frame of

the gauge boson and are explicitly given in Ref. [6] for the Collins–Soper [3] frame. In this frame the z -axis bisects the angle between \vec{P}_1 and $-\vec{P}_2$:

$$\begin{aligned}\vec{P}_1 &= E_1 (\sin \gamma_{CS}, 0, \cos \gamma_{CS}), \\ \vec{P}_2 &= E_2 (\sin \gamma_{CS}, 0, -\cos \gamma_{CS}),\end{aligned}\tag{19}$$

with

$$\cos \gamma_{CS} = \left(\frac{Q^2 S}{(T - Q^2)(U - Q^2)} \right)^{1/2} = \left(\frac{Q^2}{Q^2 + p_T^2} \right)^{1/2},\tag{20}$$

$$\sin \gamma_{CS} = -\sqrt{1 - \cos^2 \gamma_{CS}},\tag{21}$$

$$E_1 = \frac{Q^2 - T}{2\sqrt{Q^2}}, \quad E_2 = \frac{Q^2 - U}{2\sqrt{Q^2}}.\tag{22}$$

In the laboratory frame, the z -direction is defined by the proton momentum and the x -direction is defined by the transverse momentum of the gauge boson. The Lorentz transformation matrix for the boost from the laboratory frame to the CS frame is given by

$$\begin{pmatrix} E \\ p_x \\ p_y \\ p_z \end{pmatrix}_{CS} = \begin{pmatrix} \frac{Q_0}{\sqrt{Q^2}} & -\frac{p_T}{\sqrt{Q^2}} & 0 & -\frac{Q_3}{\sqrt{Q^2}} \\ -\frac{p_T Q_0}{\sqrt{Q^2} X_T} & \frac{X_T}{\sqrt{Q^2}} & 0 & \frac{p_T Q_3}{\sqrt{Q^2} X_T} \\ 0 & 0 & 1 & 0 \\ -\frac{Q_3}{X_T} & 0 & 0 & \frac{Q_0}{X_T} \end{pmatrix} \begin{pmatrix} E \\ p_x \\ p_y \\ p_z \end{pmatrix}_{lab}\tag{23}$$

where

$$X_T = \sqrt{Q^2 + p_T^2}.\tag{24}$$

Concerning the leptonic decay modes, W bosons have the disadvantage that the decay kinematics cannot be completely reconstructed due to the unobservability of the neutrino. The transverse components of the neutrino's momentum can be approximated from transverse momentum balancing in calorimetric experiments, however, the longitudinal component can only be obtained up to a twofold ambiguity. By choosing the Collins–Soper frame [3], the polar angle (θ) and the azimuthal angle (ϕ) of the charged lepton can be reconstructed

modulo a sign ambiguity in $\cos \theta$, thereby enabling the measurement of four $[\sigma^{U+L,L,T,A}]$ out of the six helicity cross sections in Eq. (14) [6]. For Z boson production and decay, ϕ and $\cos \theta$ can be determined without ambiguity.

Let us briefly review how θ and ϕ can be obtained from measured quantities in W boson production and decay. Denote the charged lepton's four-momentum in the laboratory frame by $p_l = (E_l, p_{lx}, p_{ly}, p_{lz})$ where p_{lz} and p_{lx} are the lepton's momentum components parallel and perpendicular to the proton direction in the event plane, *i.e.*, the plane spanned by the proton and the W boson with $p_T > 0$. The lepton's four-momentum in the CS frame, p_l^{CS} , can be obtained by Lorentz-boosting p_l from the laboratory frame to the CS frame. One obtains

$$\begin{aligned} p_{lx}^{CS} &= \frac{1}{2} \frac{M_W}{\sqrt{M_W^2 + p_T^2}} (2 p_{lx} - p_T) , \\ p_{ly}^{CS} &= p_{ly} , \\ p_{lz}^{CS} &= \pm \frac{M_W}{2} \left(1 - \frac{(p_{lx}^{CS})^2 + (p_{ly}^{CS})^2}{M_W^2/4} \right)^{1/2} , \end{aligned} \tag{25}$$

where the W -mass constraint has been imposed on the lepton-neutrino system. The \pm signs correspond to the two solutions for the longitudinal momentum of the neutrino. The transverse component p_{lx}^{CS} is uniquely determined by the measurable laboratory frame quantities³ p_{lx} and $p_T = p_{lx} + p_{\nu x}$. The CS frame is thus unique in the sense that in this frame the lepton's transverse momentum is independent of the unmeasured longitudinal momentum of the neutrino. On the other hand note that the longitudinal component p_{lz}^{CS} is determined only up to a sign. The angles θ and ϕ are obtained from the charged lepton's momentum components in Eq. (25) via $\phi = \arctan(p_{ly}^{CS}/p_{lx}^{CS})$ and $\theta = \arctan \sqrt{(p_{lx}^{CS})^2 + (p_{ly}^{CS})^2}/p_{lz}^{CS}$. The twofold ambiguity in the reconstruction of the lepton's longitudinal momenta in the CS frame translates into an ambiguity $\theta \leftrightarrow \pi - \theta$ in the polar angle, while ϕ is completely determined. This implies that only the helicity cross sections σ^{U+L} , σ^L , σ^T , and σ^A in Eq. (14)

³ Note that there is a misprint in the definition of p_T in Ref. [6].

can be determined in a W boson production experiment. For Z boson production, all six of the angular coefficients in Eq. (14) can be determined.

Introducing the standard angular coefficients [3]

$$\begin{aligned} A_0 &= \frac{2 d\sigma^L}{d\sigma^{U+L}}, & A_1 &= \frac{2\sqrt{2} d\sigma^I}{d\sigma^{U+L}}, & A_2 &= \frac{4 d\sigma^T}{d\sigma^{U+L}}, \\ A_3 &= \frac{4\sqrt{2} d\sigma^A}{d\sigma^{U+L}}, & A_4 &= \frac{2 d\sigma^P}{d\sigma^{U+L}}, \end{aligned} \quad (26)$$

the angular distribution in Eq. (14) can be conveniently written

$$\begin{aligned} \frac{d\sigma}{dp_T^2 dy d\cos\theta d\phi} &= \frac{3}{16\pi} \frac{d\sigma^{U+L}}{dp_T^2 dy} \left[(1 + \cos^2\theta) + \frac{1}{2}A_0 (1 - 3\cos^2\theta) \right. \\ &\quad + A_1 \sin 2\theta \cos\phi + \frac{1}{2}A_2 \sin^2\theta \cos 2\phi \\ &\quad \left. + A_3 \sin\theta \cos\phi + A_4 \cos\theta \right]. \end{aligned} \quad (27)$$

Integrating the angular distribution in Eq. (27) over the azimuthal angle ϕ yields

$$\frac{d\sigma}{dp_T^2 dy d\cos\theta} = C (1 + \alpha_1 \cos\theta + \alpha_2 \cos^2\theta), \quad (28)$$

where

$$C = \frac{3}{8} \frac{d\sigma^{U+L}}{dp_T^2 dy} \left[1 + \frac{A_0}{2} \right], \quad \alpha_1 = \frac{2A_4}{2 + A_0}, \quad \alpha_2 = \frac{2 - 3A_0}{2 + A_0}. \quad (29)$$

Integrating Eq. (27) over the polar angle θ yields

$$\frac{d\sigma}{dp_T^2 dy d\phi} = \frac{1}{2\pi} \frac{d\sigma^{U+L}}{dp_T^2 dy} (1 + \beta_1 \cos\phi + \beta_2 \cos 2\phi), \quad (30)$$

where

$$\beta_1 = \frac{3\pi}{16} A_3, \quad \beta_2 = \frac{A_2}{4}. \quad (31)$$

Before discussing numerical results, let us briefly discuss a possible strategy for extracting the angular coefficients. By taking moments with respect to an appropriate product of trigonometric functions it is possible to disentangle the coefficients A_i . A convenient definition of the moments is

$$\langle m \rangle = \frac{\int d\sigma(p_T, y, \theta, \phi) m d\cos\theta d\phi}{\int d\sigma(p_T, y, \theta, \phi) d\cos\theta d\phi}, \quad (32)$$

which leads to the following results:

$$\langle 1 \rangle = 1, \quad (33)$$

$$\langle \frac{1}{2}(1 - 3\cos^2\theta) \rangle = \frac{3}{20} \left(A_0 - \frac{2}{3} \right), \quad (34)$$

$$\langle \sin 2\theta \cos \phi \rangle = \frac{1}{5} A_1, \quad (35)$$

$$\langle \sin^2\theta \cos 2\phi \rangle = \frac{1}{10} A_2, \quad (36)$$

$$\langle \sin\theta \cos\phi \rangle = \frac{1}{4} A_3, \quad (37)$$

$$\langle \cos\theta \rangle = \frac{1}{4} A_4. \quad (38)$$

III. NUMERICAL RESULTS

In this section numerical results are presented for high p_T production and leptonic decay of W and Z bosons at the Tevatron collider center of mass energy [$\sqrt{S} = 1.8$ TeV]. The numerical results have been obtained using the MRS set D'_L [12] parton distribution functions with $\Lambda_{\overline{MS}}^{(4)} = 215$ MeV and the one-loop formula for α_s . The renormalization scale μ_R^2 and the factorization scale μ_F^2 in Eq. (7) have been taken to be $\mu_R^2 = \mu_F^2 = M_V^2 + p_T^2(V)$, where M_V and $p_T(V)$ are the mass and transverse momentum, respectively, of the gauge boson.

We begin with numerical results for the coefficients A_i in Eq. (27). These coefficients have been extracted from the Monte Carlo program by using the moments defined in Eq. (32). Figure 1(a) shows the coefficients $A_0, A_2,$ and A_3 in the CS frame as functions of $p_T(W)$ for W production. The angles θ and ϕ are the decay angles of the charged lepton in the CS frame. The results are identical for W^+ and W^- . The lepton's four-momentum in the CS frame was obtained using Eq. (25). Note that because of the ambiguity $\theta \leftrightarrow \pi - \theta$ in the polar angle reconstruction in the CS frame, the coefficients A_1 and A_4 are not observable in a W boson production experiment. However, all of the A_i coefficients are observable for

Z boson production, and the numerical results are shown in Fig. 1(b), where θ and ϕ are the angles of the negatively charged lepton. No acceptance cuts have been applied to the leptons.

The coefficients A_0 and A_2 are increasing functions of $p_T(V)$ and the deviations from the lowest order expectation of Eq. (1) [$A_0 = A_2 = 0$] are quite large, even at modest values of $p_T(V)$, *i.e.*, for $p_T(V) \approx 20 - 50$ GeV. It has been noted in Ref. [7] that these coefficients are exactly equal in LO. This is no longer true in NLO, but the corrections to A_0 and A_2 are fairly small [6]. It has been shown in Ref. [13] that the $O(\alpha_s)$ relation $A_0 = A_2$ is peculiar to a vector gluon theory. For a scalar gluon this relation is badly broken, *e.g.*, $A_0 - A_2 \approx -2$ in the Gottfried-Jackson frame at the CERN $Sp\bar{p}S$ energies. It was in fact the study of this relation in W decays by UA1 which fixed the spin of the gluon [1]. NLO numerical results for A_0 and A_2 for W decay in the Gottfried-Jackson frame are given in Ref. [14] and the deviations from $A_0 = A_2$ are found to be small. NLO numerical results for A_0 and A_2 in the CS frame are presented in Refs. [6,15].

The deviation of A_1 and A_3 from zero is much smaller, even at large $p_T(V)$. This is a special effect of the CS frame. In this frame the $q\bar{q}$ contribution in Eq. (6) to A_1 and A_3 is antisymmetric under the interchange of x_1 and x_2 ; this can be explicitly seen in the corresponding matrix elements in Eq. (24) of Ref. [6]. The qg process gives a sizable contribution to A_3 only for W boson production, and a measurement of A_3 could in principle provide constraints on the gluon distribution function⁴. However, as we will see later, experimental cuts introduce additional complicated angular effects and the resulting data sample can no longer be described by the simple angular distribution in Eq. (27). Furthermore, the extraction of the different polarization cross sections via the moments in Eq. (32) becomes problematic. Note that A_4 in Fig. 1(b) is proportional to $v_l^Z a_l^Z v_q^Z a_q^Z$ and is therefore sensitive to the Weinberg angle θ_W . This determination would be totally independent of the

⁴Note that A_3 has the wrong sign in the figures in Ref. [6]

W and Z boson masses. However, a precise determination of $\sin^2 \theta_W$ by this method is also limited by the problem of extracting A_4 with sufficient accuracy when experimental cuts are applied to the decay leptons [see the discussion below].

To give a feeling for the ϕ and $\cos \theta$ distributions of the decay leptons in the CS frame we show numerical results for the coefficients α_1, α_2 and β_1, β_2 [see Eqs. (28) and (30)] as a function of $p_T(V)$ for the W and Z boson in Fig. 2. As in Fig. 1, no cuts have been applied to the leptons. The coefficients are again very sensitive to the transverse momentum of the gauge boson. In the remainder of this paper we investigate the feasibility of using this dependence to test the polarization properties of the W and Z bosons at the Tevatron.

We want to point out that we are not in agreement with the theoretical predictions for the angular coefficients of the Z boson presented in Ref. [5] where the “soft gluon resummation” formalism was used for the integrated cross section⁵ but not for the individual helicity cross sections which are responsible for the angular distributions. Even for gauge boson transverse momenta larger than $p_T > 20$ GeV, where the angular coefficients should be reliably predicted by fixed order perturbative QCD, our predictions differ dramatically from the results in Ref. [5], for example, by a factor five for the coefficient A_0 in Eq. (27) at $p_T(Z) = 60$ GeV. The complete NLO calculation in Ref. [6] for the helicity cross sections shows that the deviations from the LO result are much smaller than the predictions in Ref. [5].

Figures 3–13 show the normalized ϕ and $\cos \theta$ distributions for the leptons from the decay of W and Z bosons for four bins in the transverse momentum of the gauge boson. To demonstrate the effects of acceptance cuts, results are shown first without cuts and then with typical acceptance cuts imposed on the leptons. The acceptance cuts are necessary to reduce the background from low p_T jets which can fake electrons. They are also needed due

⁵The integrated cross section is essentially the total cross section after integration over θ and ϕ , *i.e.*, σ^{U+L} in Eq. (14).

to the finite acceptance of the detector. Measurements of the charged lepton momentum and the missing transverse momentum \cancel{p}_T have inherent uncertainties due to the finite energy resolution of the detector. These uncertainties have been simulated in our calculation by Gaussian smearing of the charged lepton and neutrino four-momentum vectors with standard deviation σ . The numerical results presented here were made using σ values based on the CDF specifications [16]. The energy resolution smearing has a non-negligible effect only on the $\cos\theta$ distribution of the charged lepton from W decay.

Figure 3 shows the ϕ and $\cos\theta$ distributions for the W boson without cuts or smearing. The curves in Fig. 3 can be obtained from α_2 , β_1 , and β_2 in Fig. 2. For example, in the lowest $p_T(W)$ bin [solid curve], the ϕ distribution is almost flat [$\beta_1, \beta_2 \approx 0$] and the $\cos\theta$ distribution is approximately $1 + \cos^2\theta$ [$\alpha_2 \approx 1$]. In the highest $p_T(W)$ bin [dot-dashed curve], one observes the ϕ dependence [$\beta_1, \beta_2 \neq 0$] resulting from the non-diagonal elements of the spin-density matrix of the W boson, whereas the corresponding $\cos\theta$ distribution is almost flat [$\alpha_2 \approx 0$]. Note that if the W boson was to decay isotropically, the ϕ and $\cos\theta$ distributions would both be flat.

Figure 4 shows the ϕ and $\cos\theta$ distributions for the W boson for the same bins in $p_T(W)$ as in Fig. 3, but with energy resolution smearing and the cuts

$$p_T(l) > 25 \text{ GeV}, \quad \cancel{p}_T > 25 \text{ GeV}, \quad y(l) < 1. \quad (39)$$

Only 33% of the events pass the cuts in Eq. (39). The cuts have a dramatic effect on the shapes of the distributions. The shapes of the distributions are now governed by the kinematics of the surviving events. The cuts, which are applied in the laboratory frame, introduce a strong ϕ dependence. The “kinematical” ϕ distribution in Fig. 4(a) is very different from the “dynamical” ϕ distribution in Fig. 3(a). The only remaining vestiges of the polarization effects in the ϕ distribution are the dips in the high $p_T(W)$ curve [dot-dashed curve] at $\phi = 90^\circ, 180^\circ, \text{ and } 270^\circ$.

The $\cos\theta$ distributions with cuts in Fig. 4(b) are very different from the corresponding results without cuts or smearing in Fig. 3(b). In order to separate the effects of smearing

from the effects of cuts, the $\cos\theta$ distribution is shown in Fig. 5 with the cuts of Eq. (39), but without smearing. The main effect of the cuts is to remove events with $\cos\theta > 0.5$ for small values of $p_T(W)$, causing the curves to drop to zero as $\cos\theta \rightarrow 1$ [see the solid and dashed curves in Fig. 5]. Comparing Figs. 4(b) and 5, we see that the smearing of the lepton momentum and the missing transverse momentum has a large effect on the $\cos\theta$ distribution in the small $\cos\theta$ region. This behavior of the smeared curves can be traced to the expression for $p_{l_z}^{CS}$ in Eq. (25). Small values of $\cos\theta$ correspond to small values of $p_{l_z}^{CS}$. When events with small values of $\cos\theta$ are smeared, the argument of the square root function in the expression for $p_{l_z}^{CS}$ often becomes negative, in which case the argument is set equal to zero in the Monte Carlo program. Thus many events with small values of $\cos\theta$ are smeared such that they end up in the $\cos\theta = 0$ bin, which is not shown here since it is off the vertical scale. When cuts and smearing are combined, as in Fig. 4(b), very little polarization dependence is left in the $\cos\theta$ distribution for the W boson.

We have also analyzed the effect of the cuts separately by using the correct matrix element for W boson production, but with isotropic decay of the W boson, *i.e.*, neglecting spin correlations between W production and decay. The angular distributions in this case are very similar to the ones shown in Fig. 4 for the full matrix element; the remnant polarization effects discussed in Fig. 4 are of course absent. In Fig. 6 we show ratios of the ϕ and $\cos\theta$ distributions for the same bins in $p_T(W)$ as in Figs. 3–5; the distribution with full polarization has been divided by the distribution obtained with isotropic decay of the W boson. Cuts and smearing are included in both cases. The large effects from the cuts and smearing are expected to almost cancel in this ratio. In fact, we nearly recover the ϕ and $\cos\theta$ dependence of Fig. 3 which contains no cuts or smearing. Therefore, to regain sensitivity to the polarization effects in the presence of large kinematic cuts, we propose to divide the experimental distributions by the Monte Carlo distributions obtained using isotropic gauge boson decay.

Figure 7 again shows the ϕ and $\cos\theta$ distributions for the W boson with energy resolution smearing, but now with the looser cuts

$$p_T(l) > 15 \text{ GeV}, \quad \not{p}_T > 15 \text{ GeV}, \quad y(l) < 2.5. \quad (40)$$

The results now display more of the polarization effects seen in Fig. 3. The dips in the ϕ distribution in the high $p_T(W)$ curve [dot-dashed curve] at $\phi = 90^\circ$ and 270° in Fig. 7(a) are much more distinctive than in Fig. 4(a). Dynamical effects in the $\cos\theta$ distribution [see Fig. 3(b)] can still be observed in Fig. 7(b) for $\cos\theta$ values in the range $0.3 < \cos\theta < 0.8$. Figure 8 shows the ratio of the “polarized” ϕ and $\cos\theta$ distributions to the corresponding distributions with isotropic leptonic decay for the cuts in Eq. (40). Most of the polarization dependence seen in Fig. 3 is retained in this ratio.

The ϕ and $\cos\theta$ distributions of the leptons from Z boson decay are shown in Figs. 9–13 for four bins in $p_T(Z)$. For Z bosons, the lepton momenta in the CS frame can be obtained from the measured lepton momenta in the laboratory frame by applying the boost matrix given in Eq. (23). The ϕ and $\cos\theta$ distributions of the negatively charged lepton are shown without cuts in Fig. 9. Again, there are large differences between the different $p_T(Z)$ bins. If the electric charge of the lepton can be determined, then the coefficient A_4 [or α_1] can in principle be measured and the $\cos\theta$ distribution in Fig. 9(b) is asymmetric about $\cos\theta = 0$. However, if the lepton’s electric charge can not be determined, the term linear in $\cos\theta$ will be averaged out, and the resulting $\cos\theta$ distribution will be symmetric.

Figure 10 shows the ϕ and $\cos\theta$ distributions for the Z boson using the same bins in $p_T(Z)$ as in Fig. 9, but now with energy resolution smearing and the cuts

$$p_T(l) > 25 \text{ GeV}, \quad y(l) < 1. \quad (41)$$

Note that these cuts are more stringent than the cuts for the W boson in Eq. (39) since now both leptons must be in the central rapidity region. The effect of the energy resolution smearing is negligible for the Z boson. The cuts introduce a ϕ dependence similar to that discussed for the W boson case in Fig. 4(a). Some polarization effects are still observable in the ϕ distribution in the high $p_T(Z)$ bins, for example, the dip in the dot-dashed curve and the flat behavior in the dotted curve around $\phi = 90^\circ$ and 270° in Fig. 10(a) are due to polarization effects.

The cuts in Eq. (41) have an even more dramatic effect on the $\cos\theta$ distribution. Since nearly all events with $|\cos\theta| > 0.6$ are rejected, almost all sensitivity to the asymmetry in Fig. 9(b) is lost. Furthermore, the curves in Fig. 10(b) are fairly similar in shape. Therefore it may be very difficult to observe any polarization effect from the Z boson in these distributions when the cuts in Eq. (41) are imposed. However, by forming the ratio of the ϕ and $\cos\theta$ distributions with full polarization to the corresponding distributions obtained with isotropic Z decay, most of the polarization dependence is recovered; see Fig. 11.

Since the experimental signature of the Z boson decay is much cleaner than that for the W boson, Fig. 12 shows the ϕ and $\cos\theta$ distributions for the Z boson for the looser cuts

$$p_T(l) > 10 \text{ GeV}, \quad y(l) < 2.5. \quad (42)$$

The large dips in the ϕ distribution in the high $p_T(Z)$ bin [dot-dashed curve] at $\phi = 90^\circ$ and 270° are due to polarization effects [compare Fig. 12(a) to Fig. 9(a)]. The curves in the central region of $\cos\theta$ in Fig. 12(b) now clearly exhibit the polarization effects seen in the corresponding curves in Fig. 9(b). Finally, Fig. 13 shows the ratio of the “polarized” ϕ and $\cos\theta$ distributions to the corresponding distributions obtained with isotropic leptonic decay for the Z boson for the cuts in Eq. (42). The ratios once again contain most of the polarization dependence seen in Fig. 9.

IV. SUMMARY

The polar and azimuthal angular distributions of the lepton pair arising from the decay of a W or Z boson produced at high transverse momentum in hadronic collisions have been discussed. In the absence of cuts on the final state leptons, the general structure of the lepton angular distribution in the gauge boson rest frame is determined by the gauge boson polarization. At $\mathcal{O}(\alpha_s)$ in perturbative QCD, the structure is described by six helicity cross sections, which are functions of the transverse momentum and rapidity of the gauge boson.

We have studied the angular distributions of the leptonic decay products of high p_T gauge bosons when acceptance cuts and energy resolution smearing are applied to the lep-

tons. When acceptance cuts are imposed on the leptons, the shapes of the lepton angular distributions are dominated by kinematic effects and the residual dynamical effects from the gauge boson polarization are small. The kinematic effects become more dominant as the cuts become more stringent. Energy resolution smearing has a significant effect only on the $\cos\theta$ distribution from W decay. The large smearing effect in this distribution is a consequence of the undetermined longitudinal momentum of the neutrino. The angular distributions have been calculated in the Collins-Soper frame. For W decay, this frame has the unique advantage that the polar and azimuthal angles θ and ϕ can be reconstructed modulo a sign ambiguity in $\cos\theta$ without information on the longitudinal momentum of the neutrino.

When cuts are imposed on the leptons, the only polarization effects visible in the ϕ and $\cos\theta$ distributions occur at large values of the gauge boson transverse momentum, where unfortunately, the cross section is smallest. Polarization effects can be maximized by minimizing the cuts, however, this strategy is severely limited since cuts are needed to reject background events. Alternatively, it may be possible to highlight gauge boson polarization effects by “dividing out” the kinematic effects, *i.e.*, if the histogrammed data is divided by the theoretical result for isotropic gauge boson decay, the resulting ratio is more sensitive to polarization effects.

Since polarization effects are nearly obscured by the kinematical effect of cuts, experimental analyses of the very small so-called “T-odd” effects discussed in Ref. [6] or possible CP violation effects in the Standard Model through the Kobayashi-Maskawa mechanism in hadronic W and Z production [17] appear to be impractical in the presence of realistic cuts at the Tevatron.

Acknowledgements

We thank V. Barger, F. Halzen, and D. Summers for useful discussions. This work is supported in part by the U.S. Department of Energy under contract Nos. DE-AC02-76ER00881 and DE-FG03-91ER40674, by Texas National Research Laboratory Grant No. RGFY93-330,

and by the University of Wisconsin Research Committee with funds granted by the Wisconsin Alumni Research Foundation.

FIGURE CAPTIONS

Fig. 1 a) Angular coefficients $A_0, A_2,$ and A_3 for W boson production and decay in the CS frame as a function of the transverse momentum $p_T(W)$ at $\sqrt{S} = 1.8$ TeV.

b) Angular coefficients $A_0, A_1, A_2, A_3,$ and A_4 for Z boson production and decay in the CS frame as a function of the transverse momentum $p_T(Z)$ at $\sqrt{S} = 1.8$ TeV.

No cuts or smearing have been applied.

Fig. 2 a) Angular coefficients $\alpha_2, \beta_1,$ and β_2 for W boson production and decay in the CS frame as a function of the transverse momentum $p_T(W)$ at $\sqrt{S} = 1.8$ TeV.

b) Angular coefficients $\alpha_1, \alpha_2, \beta_1,$ and β_2 for Z boson production and decay in the CS frame as a function of the transverse momentum $p_T(Z)$ at $\sqrt{S} = 1.8$ TeV.

No cuts or smearing have been applied.

Fig. 3 a) Normalized ϕ and b) normalized $\cos\theta$ distributions of the charged lepton from W boson decay in the CS frame. Results are shown for four bins in $p_T(W)$:

10 GeV $< p_T(W) < 20$ GeV (solid),

20 GeV $< p_T(W) < 30$ GeV (dashed),

30 GeV $< p_T(W) < 70$ GeV (dots),

70 GeV $< p_T(W)$ (dot-dashed).

No cuts or smearing have been applied.

Fig. 4 Same as Fig. 3 but with smearing and the cuts $p_T(l) > 25$ GeV, $p_T^l > 25$ GeV, and $y(l) < 1$.

Fig. 5 Normalized $\cos\theta$ distribution of the charged lepton from W boson decay in the CS frame. The cuts $p_T(l) > 25$ GeV, $p_T^l > 25$ GeV, and $y(l) < 1$ have been imposed, but no smearing is included.

Fig. 6 Ratios of distributions obtained with full polarization effects to those obtained with isotropic decay of the W boson. Parts a) and b) are the ratios for the ϕ and $\cos\theta$

distributions, respectively. Energy resolution smearing and the cuts $p_T(l) > 25$ GeV, $\cancel{p}_T > 25$ GeV, and $y(l) < 1$ are included.

Fig. 7 Same as Fig. 3 but with smearing and the cuts $p_T(l) > 15$ GeV, $\cancel{p}_T > 15$ GeV, and $y(l) < 2.5$.

Fig. 8 Same as Fig. 6 but with the cuts $p_T(l) > 15$ GeV, $\cancel{p}_T > 15$ GeV, and $y(l) < 2.5$.

Fig. 9 a) Normalized ϕ and b) normalized $\cos \theta$ distributions of the negatively charged lepton from Z boson decay in the CS frame. Results are shown for four bins in $p_T(Z)$:

10 GeV $< p_T(Z) < 20$ GeV (solid),

20 GeV $< p_T(Z) < 30$ GeV (dashed),

30 GeV $< p_T(Z) < 70$ GeV (dots),

70 GeV $< p_T(Z)$ (dot-dashed).

No cuts or smearing have been applied.

Fig. 10 Same as Fig. 9 but with smearing and the cuts $p_T(l) > 25$ GeV and $y(l) < 1$.

Fig. 11 Ratios of distributions obtained with full polarization effects to those obtained with isotropic decay of the Z boson. Parts a) and b) are the ratios for the ϕ and $\cos \theta$ distributions, respectively. Energy resolution smearing and the cuts $p_T(l) > 25$ GeV and $y(l) < 1$ are included.

Fig. 12 Same as Fig. 9 but with smearing and the cuts $p_T(l) > 10$ GeV and $y(l) < 2.5$.

Fig. 13 Same as Fig. 11 but with the cuts $p_T(l) > 10$ GeV and $y(l) < 2.5$.

REFERENCES

- [1] C. Albajar *et al.* (UA1 collaboration), *Z. Phys.* **C 44** (1989) 15.
- [2] R. Ansari *et al.* (UA2 collaboration), *Phys. Lett.* **B 186** (1987) 440.
- [3] J. C. Collins and D. E. Soper, *Phys. Rev.* **D 16** (1977) 2219.
- [4] M. Chaichian, M. Hayashi, and K. Yamagishi, *Phys. Rev.* **D 25** (1982) 130.
- [5] P. Chiappetta and M. Le Bellac, *Z. Phys.* **C 32** (1986) 521;
P. Chiappetta and J. Ph. Guillet, *Phys. Lett.* **B 233** (1989) 256.
- [6] E. Mirkes, *Nucl. Phys.* **B 387** (1992) 3.
- [7] C. S. Lam and W.-K. Tung, *Phys. Rev.* **D 18** (1978) 2447;
ibid. **D 21** (1980) 2712; *Phys. Lett.* **B 80** (1979) 228;
K. Kajantie, J. Lindfors, and R. Raitio, *Phys. Lett.* **B 74** (1978) 384;
Nucl. Phys. **B 144** (1978) 422;
J. Cleymans and M. Kuroda, *Phys. Lett.* **B 80** (1979) 385;
Nucl. Phys. **B 155** (1979) 480;
R. L. Thews, *Phys. Rev. Lett.* **43** (1979) 987;
J. Lindfors, *Phys. Scr.* **20**, (1979), 19.
- [8] F. Halzen and D. M. Scott, *Phys. Lett.* **B 78** (1978) 318;
F. Halzen, A. D. Martin, and D. M. Scott, *Phys. Rev.* **D 25** (1982) 754;
P. Aurenche and J. Lindfors, *Nucl. Phys.* **B 185** (1981) 274; *ibid.* **B 185** (1981) 301.
- [9] S. Falciano *et al.* (NA10 collaboration), *Z. Phys.* **C 31** (1986) 513;
M. Guanziroli *et al.* (NA10 collaboration), *ibid.* **C 37** (1988) 545;
J. S. Conway *et al.*, *Phys. Rev.* **D 39** (1989) 92;
J. G. Heinrich *et al.*, *ibid.* **D 44** (1991) 44.
- [10] A. Brandenburg, O. Nachtmann, and E. Mirkes, *Z. Phys.* **C 60** (1993) 697;

- A. Brandenburg, S. J. Brodsky, V. V. Khoze, and D. Müller, SLAC-PUB-6464, (1994).
- [11] K. Hagiwara, K. Hikasa, and N. Kai, *Phys. Rev. Lett.* **52** (1984) 1076.
- [12] A. D. Martin, R. G. Roberts, and W. J. Stirling, *Phys. Lett.* **B 306** (1993) 145.
- [13] N. Arteaga-Romero, A. Nicolaidis, and J. Silva, *Phys. Rev. Lett.* **52** (1984) 172.
- [14] E. Mirkes, Proc. of the XXVIth Rencontre de Moriond '91 High Energy Hadronic Interactions, p. 81.
- [15] E. Mirkes, J. G. Körner, and G. A. Schuler, *Phys. Lett.* **B 259** (1991) 151.
- [16] F. Abe *et al.* (CDF collaboration), *Phys. Rev.* **D 45** (1992) 3921.
- [17] A. Brandenburg, J. P. Ma, R. Münch, and O. Nachtmann, *Z. Phys.* **C 51** (1991) 225;
A. Brandenburg, J. P. Ma, and O. Nachtmann, *ibid.* **C 55** (1992) 115.

This figure "fig1-1.png" is available in "png" format from:

<http://arXiv.org/ps/hep-ph/9406381v1>

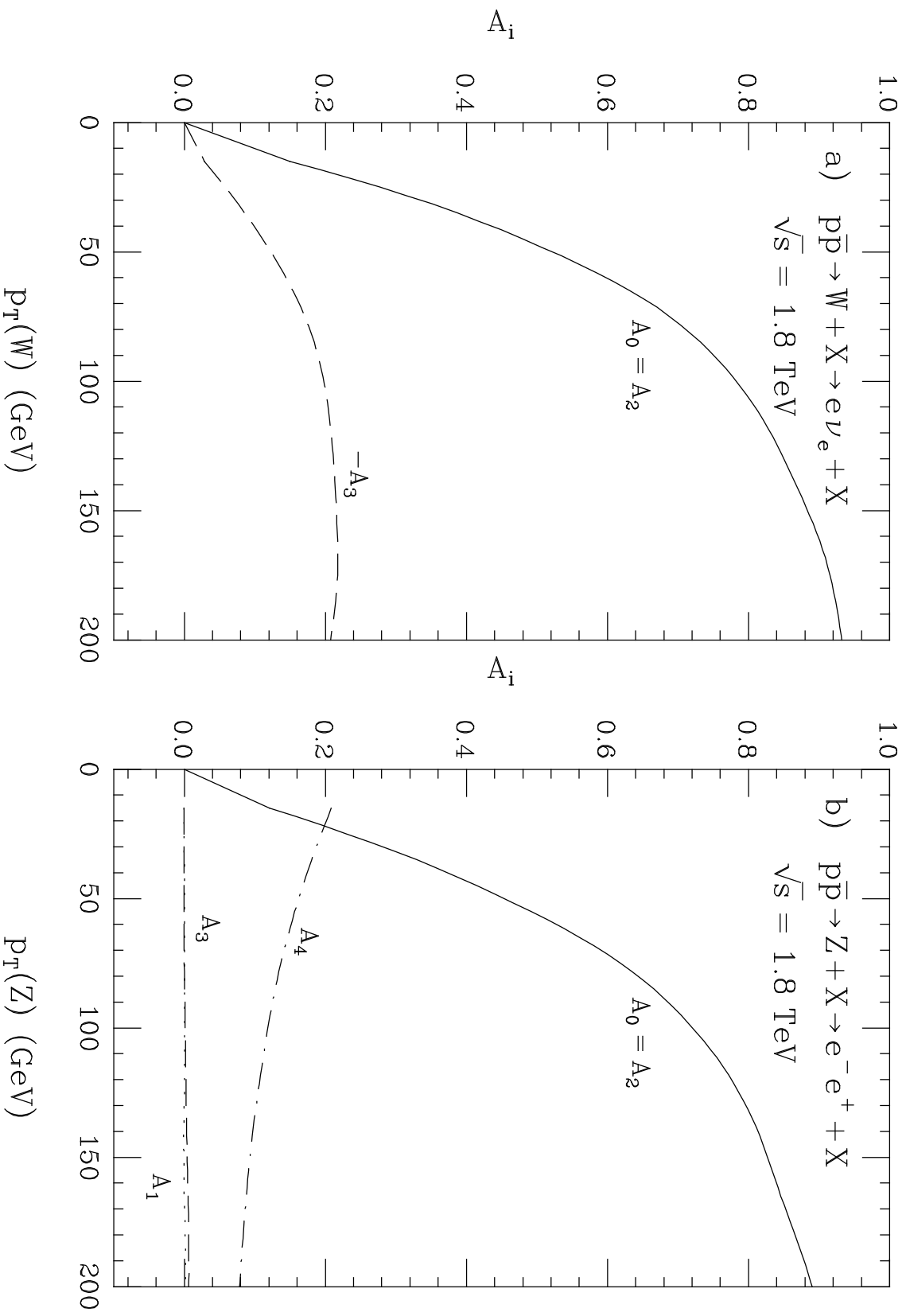


Figure 1

This figure "fig2-1.png" is available in "png" format from:

<http://arXiv.org/ps/hep-ph/9406381v1>

This figure "fig3-1.png" is available in "png" format from:

<http://arXiv.org/ps/hep-ph/9406381v1>

This figure "fig1-2.png" is available in "png" format from:

<http://arXiv.org/ps/hep-ph/9406381v1>

This figure "fig2-2.png" is available in "png" format from:

<http://arXiv.org/ps/hep-ph/9406381v1>

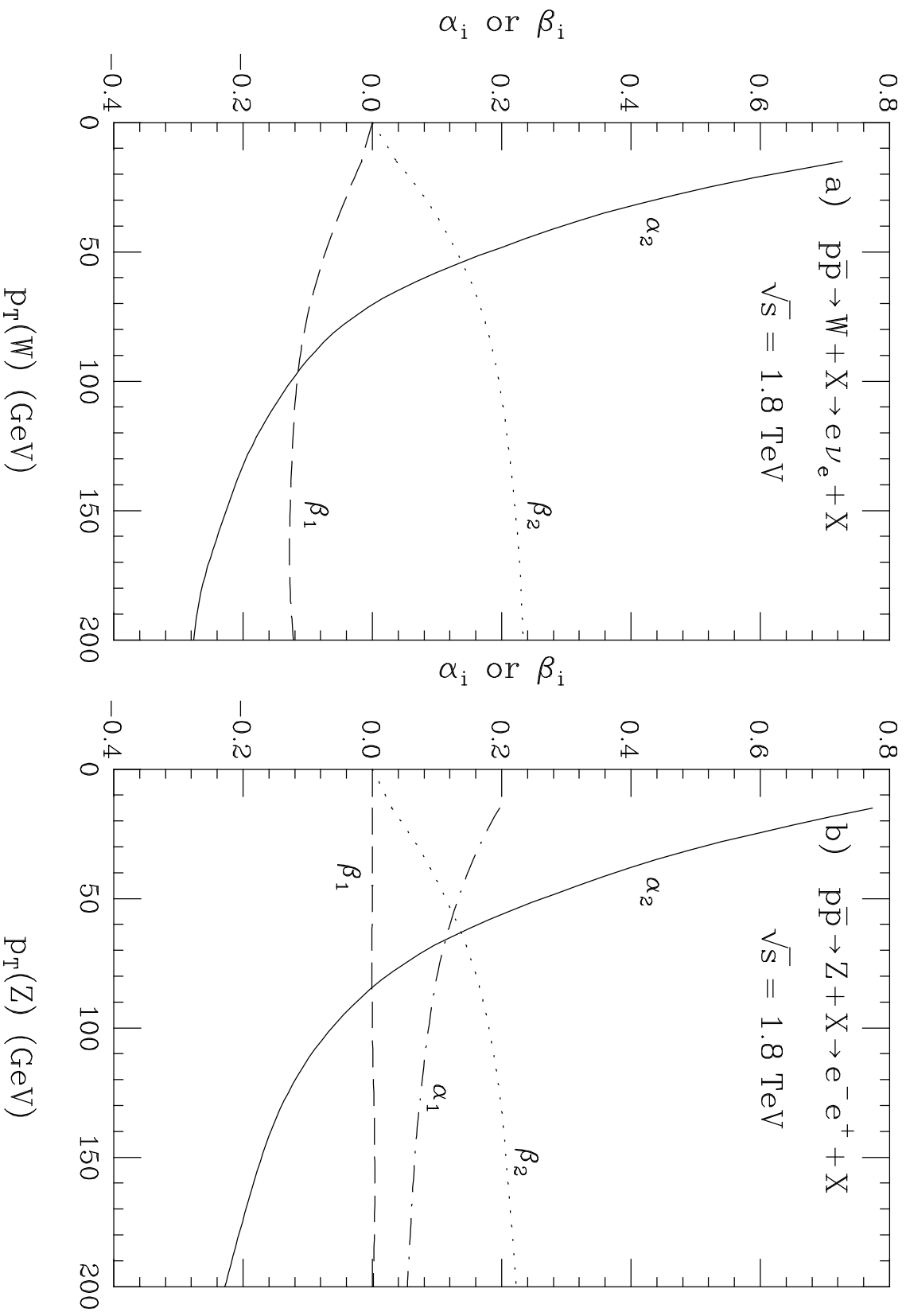


Figure 2

This figure "fig3-2.png" is available in "png" format from:

<http://arXiv.org/ps/hep-ph/9406381v1>

This figure "fig1-3.png" is available in "png" format from:

<http://arXiv.org/ps/hep-ph/9406381v1>

This figure "fig2-3.png" is available in "png" format from:

<http://arXiv.org/ps/hep-ph/9406381v1>

This figure "fig3-3.png" is available in "png" format from:

<http://arXiv.org/ps/hep-ph/9406381v1>

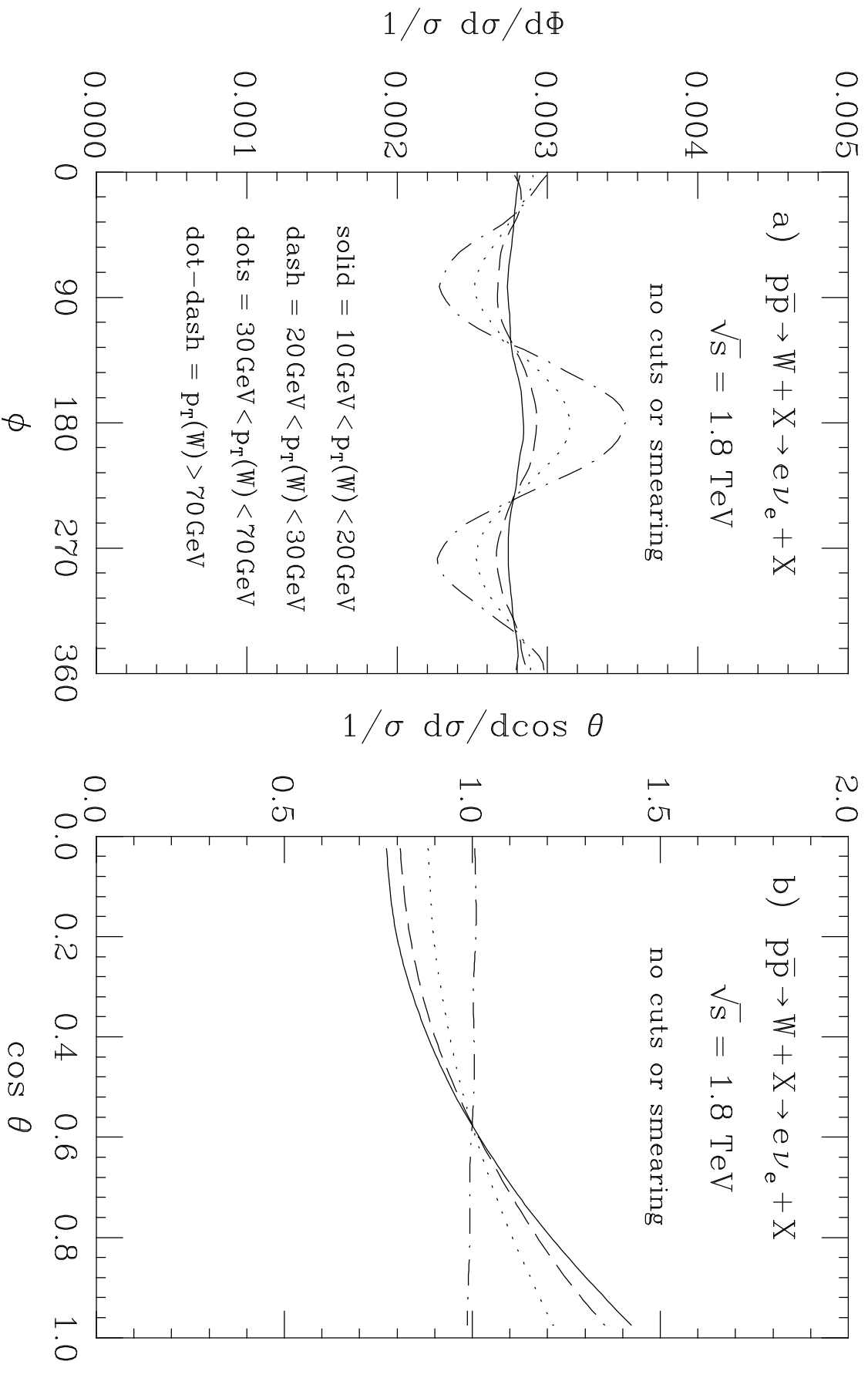


Figure 3

This figure "fig1-4.png" is available in "png" format from:

<http://arXiv.org/ps/hep-ph/9406381v1>

This figure "fig2-4.png" is available in "png" format from:

<http://arXiv.org/ps/hep-ph/9406381v1>

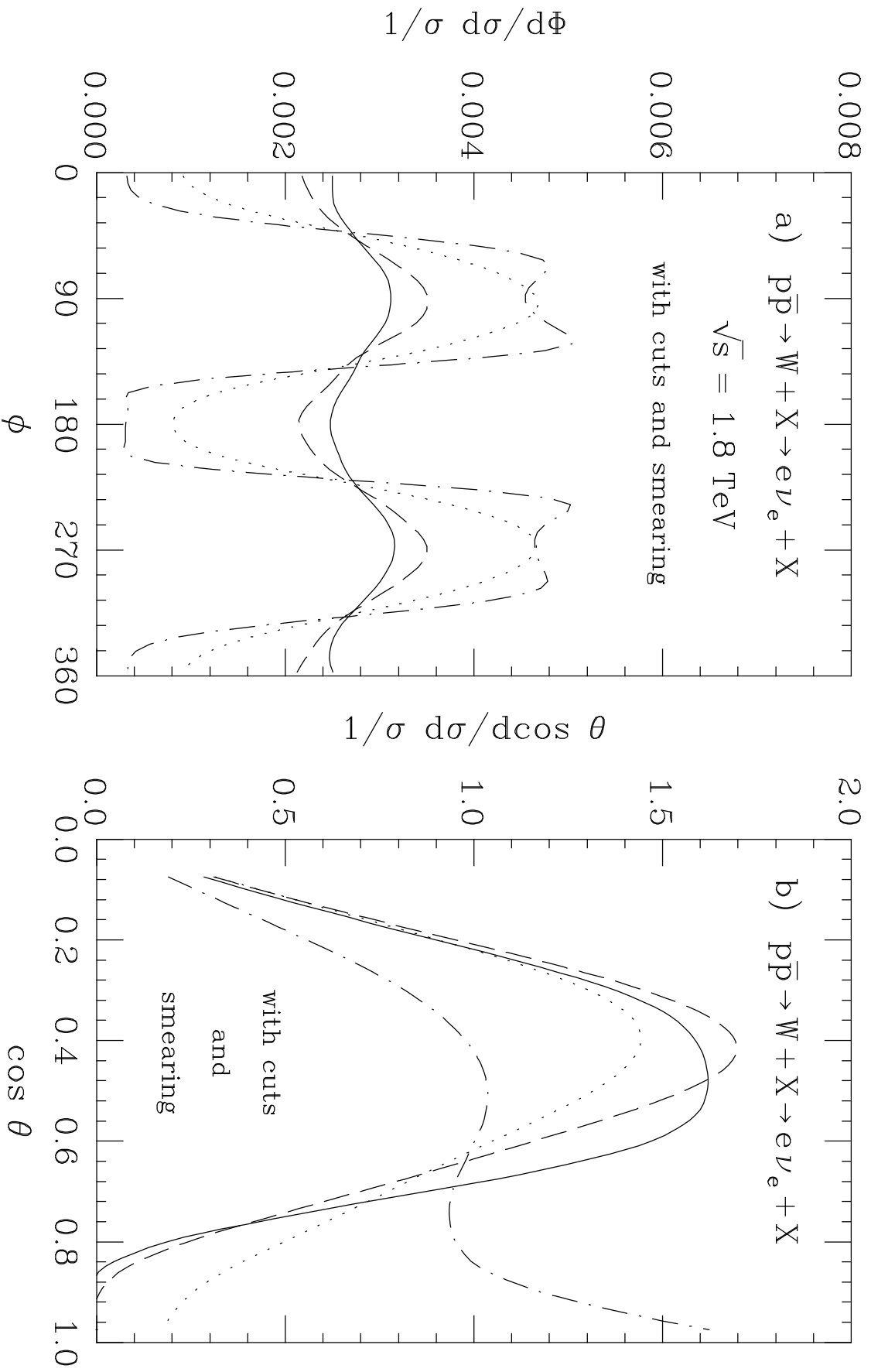


Figure 4

This figure "fig1-5.png" is available in "png" format from:

<http://arXiv.org/ps/hep-ph/9406381v1>

This figure "fig2-5.png" is available in "png" format from:

<http://arXiv.org/ps/hep-ph/9406381v1>

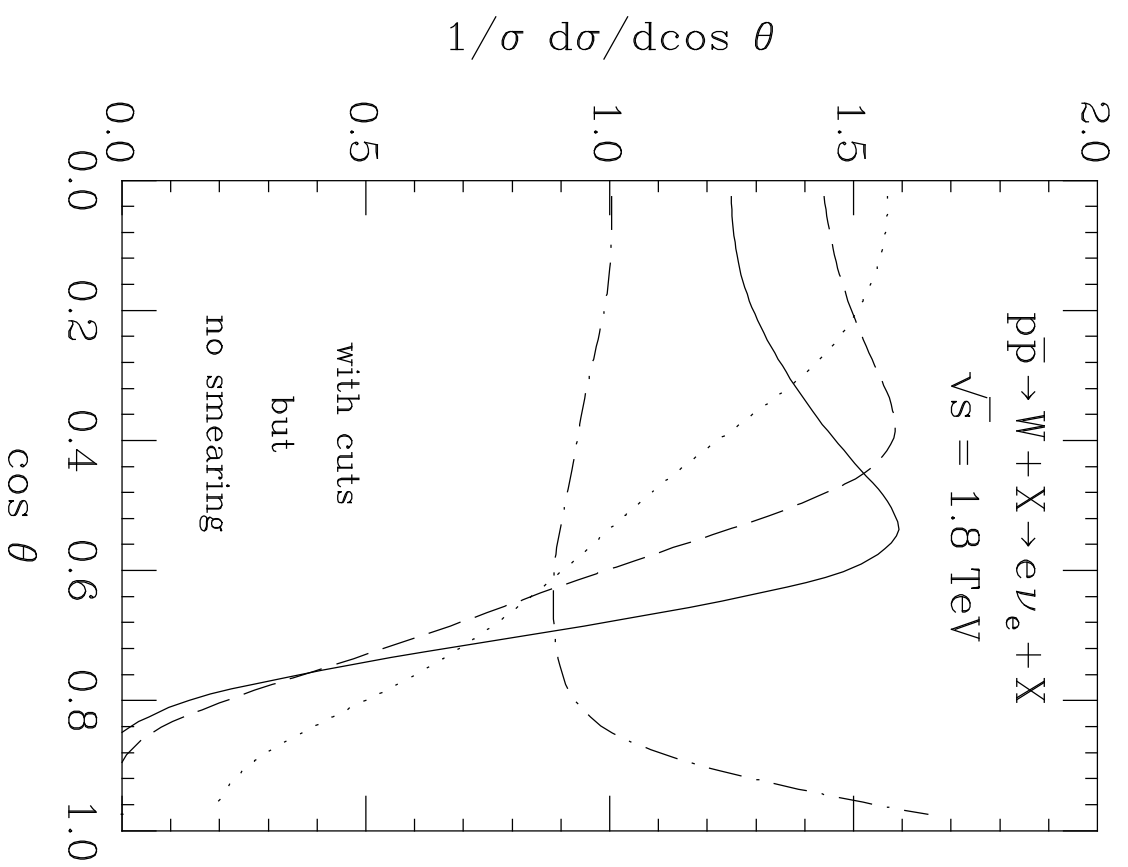


Figure 5

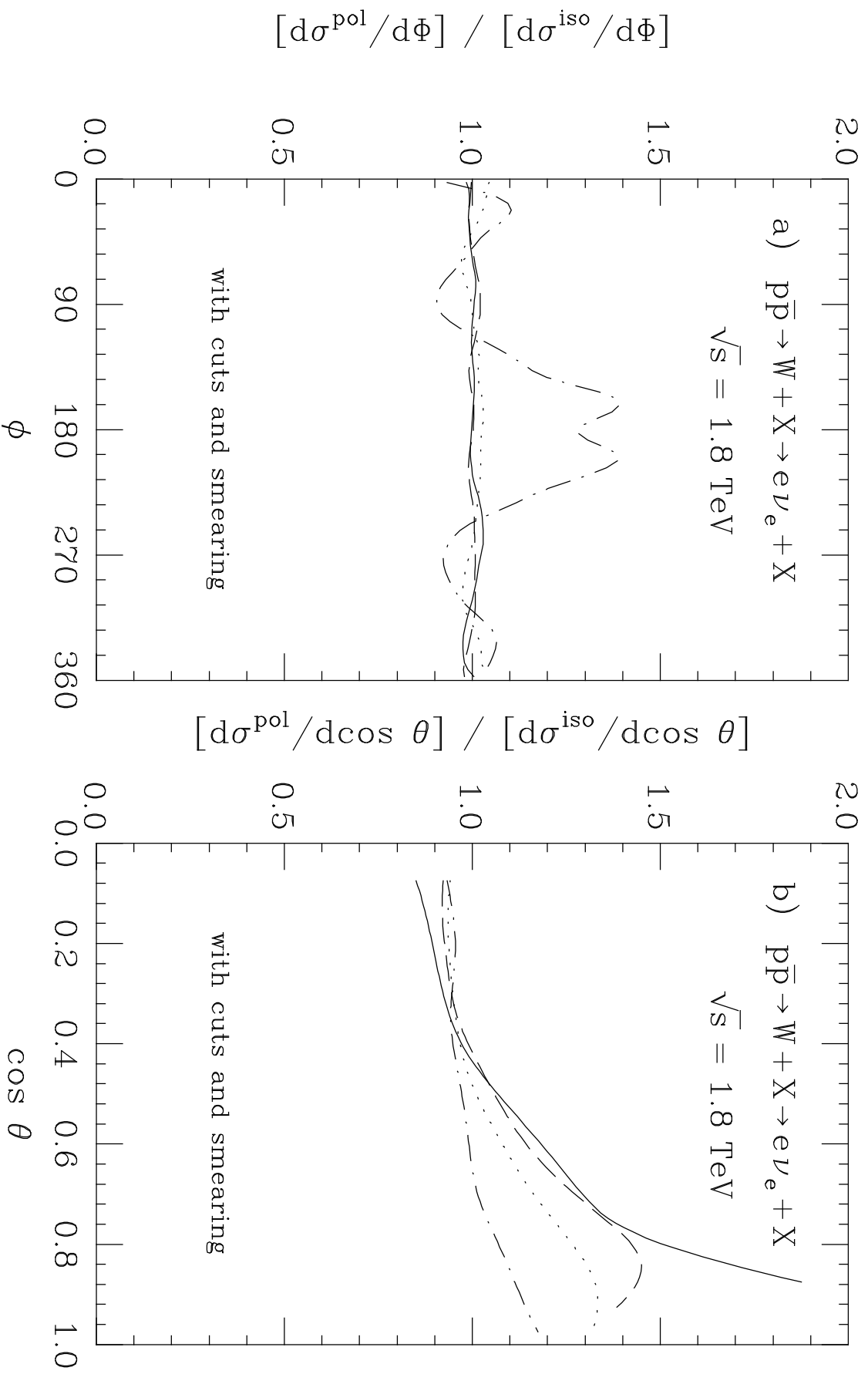


Figure 6

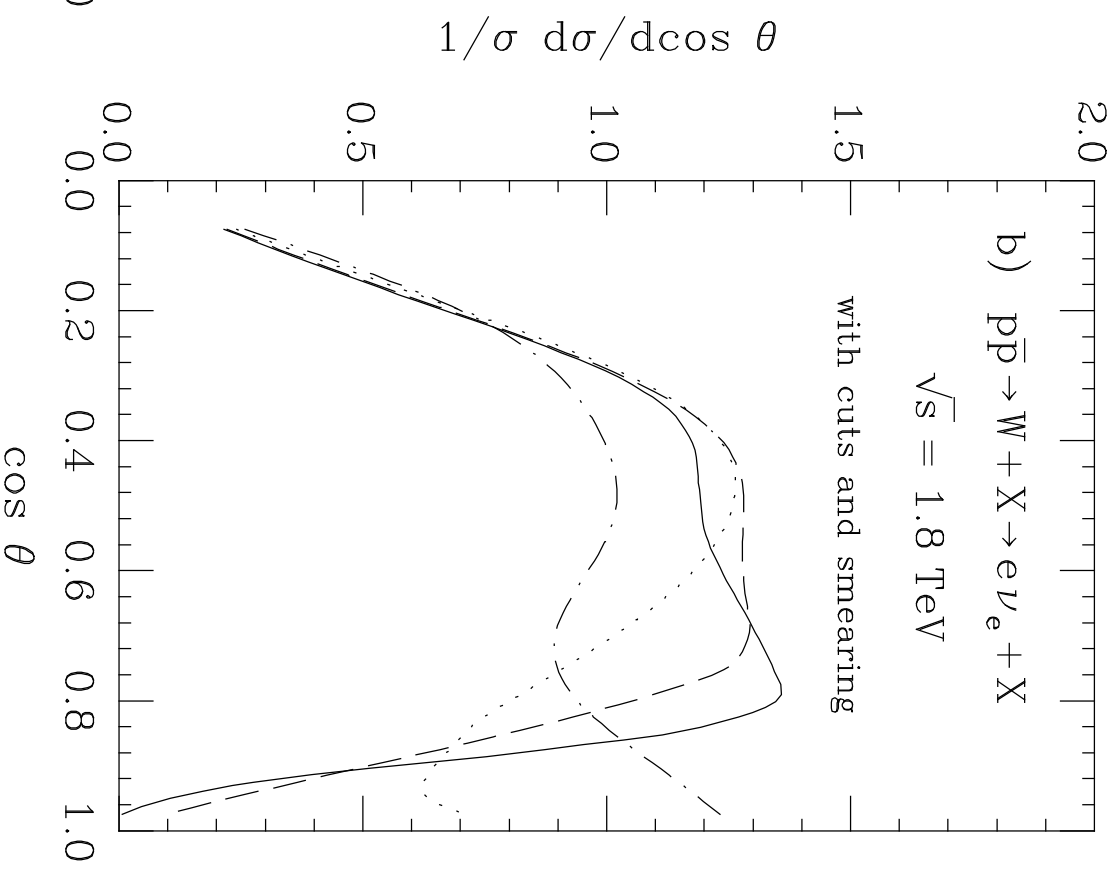
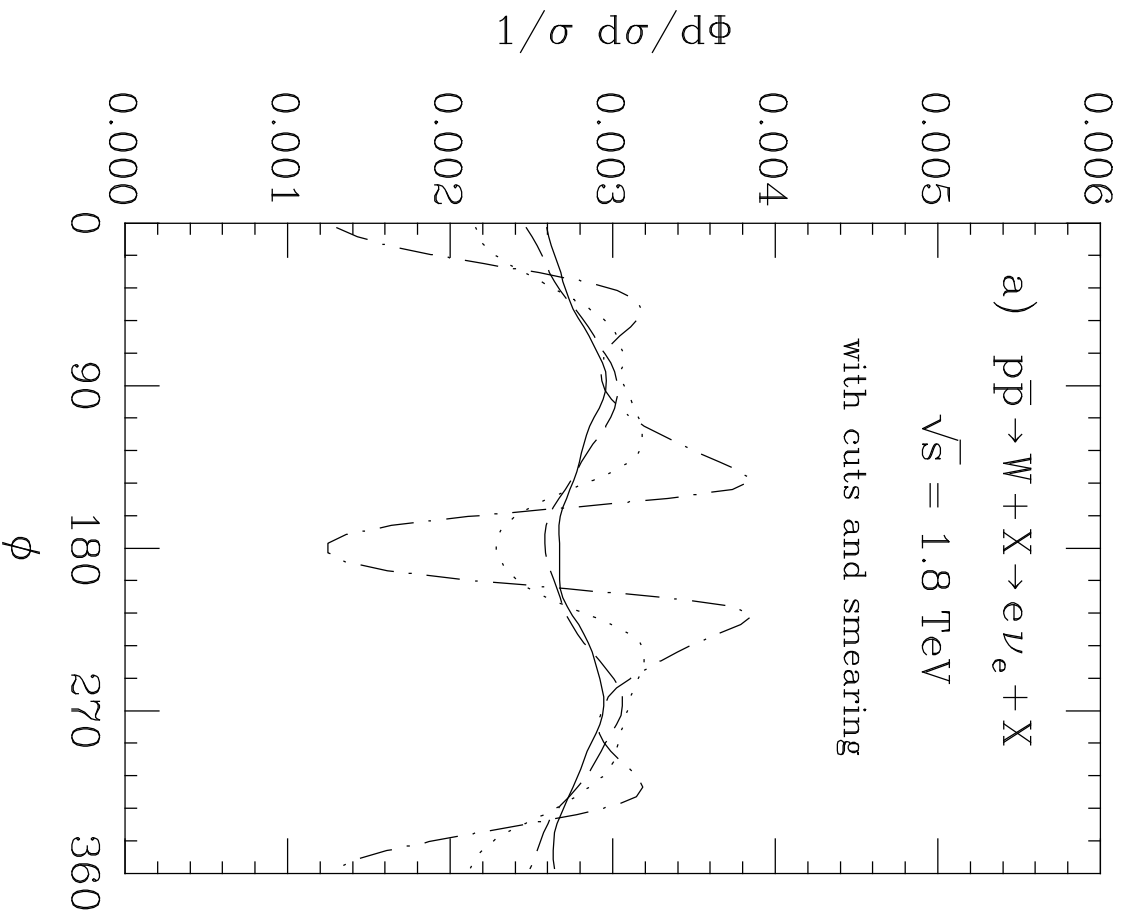


Figure 7

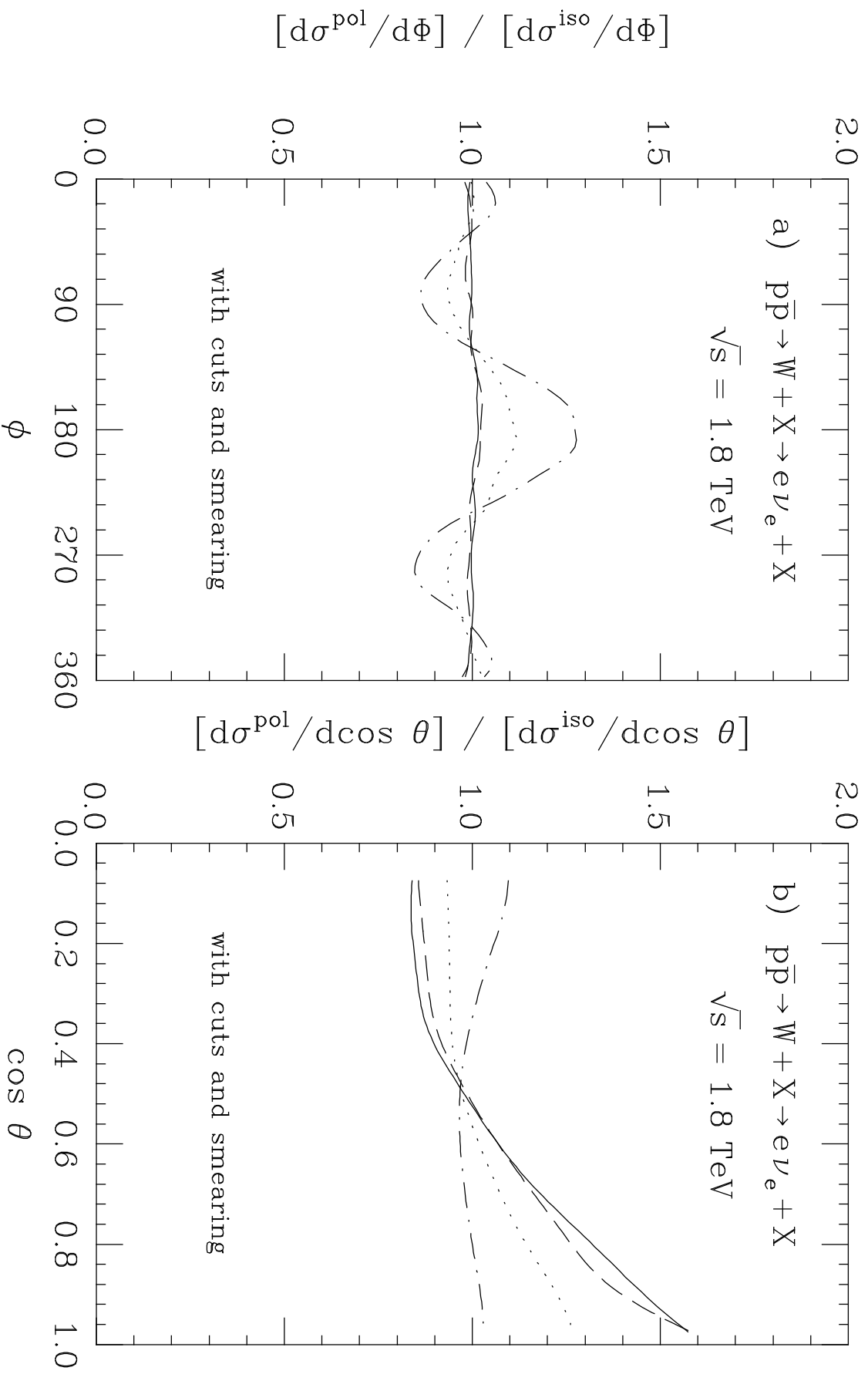


Figure 8

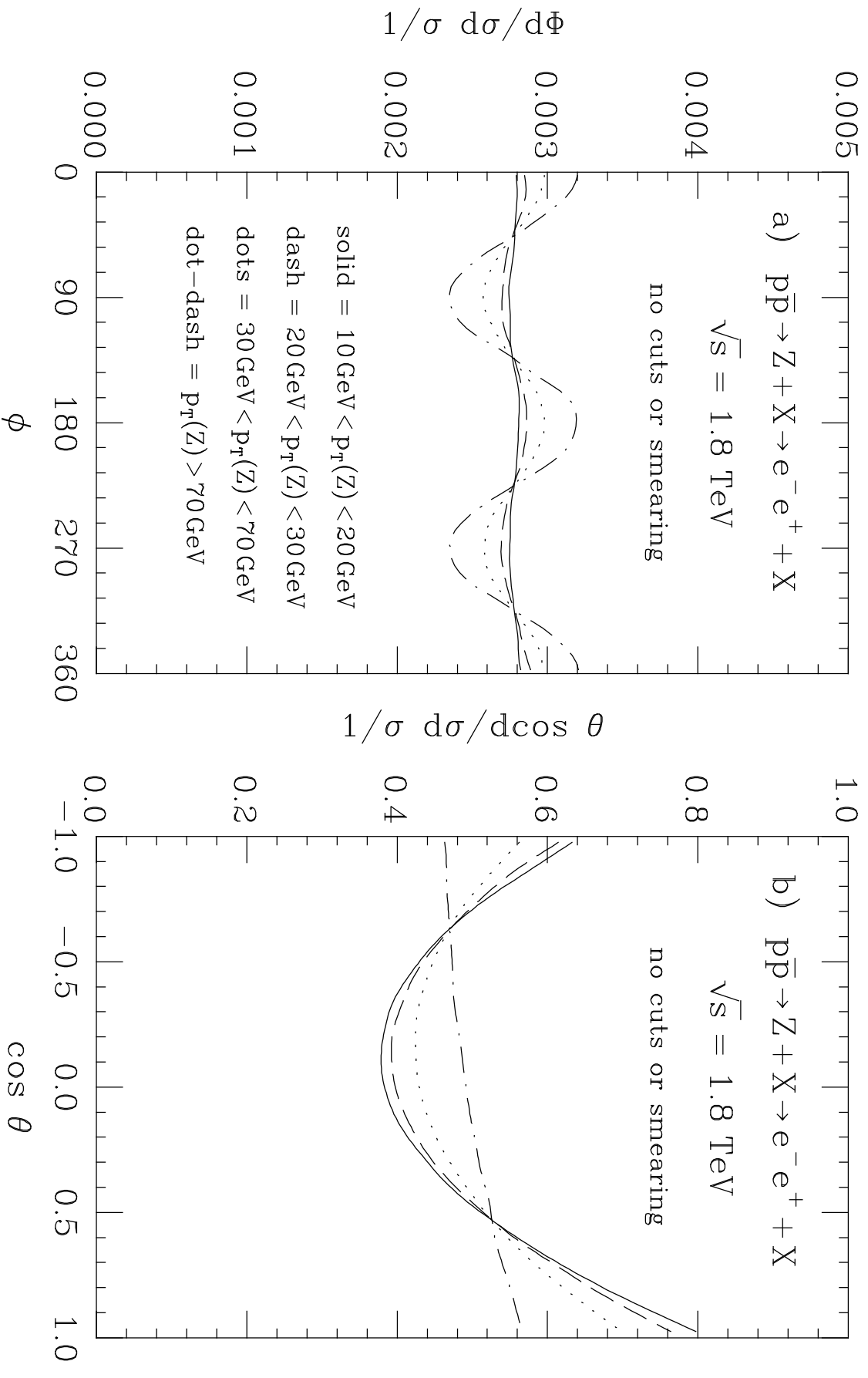


Figure 9

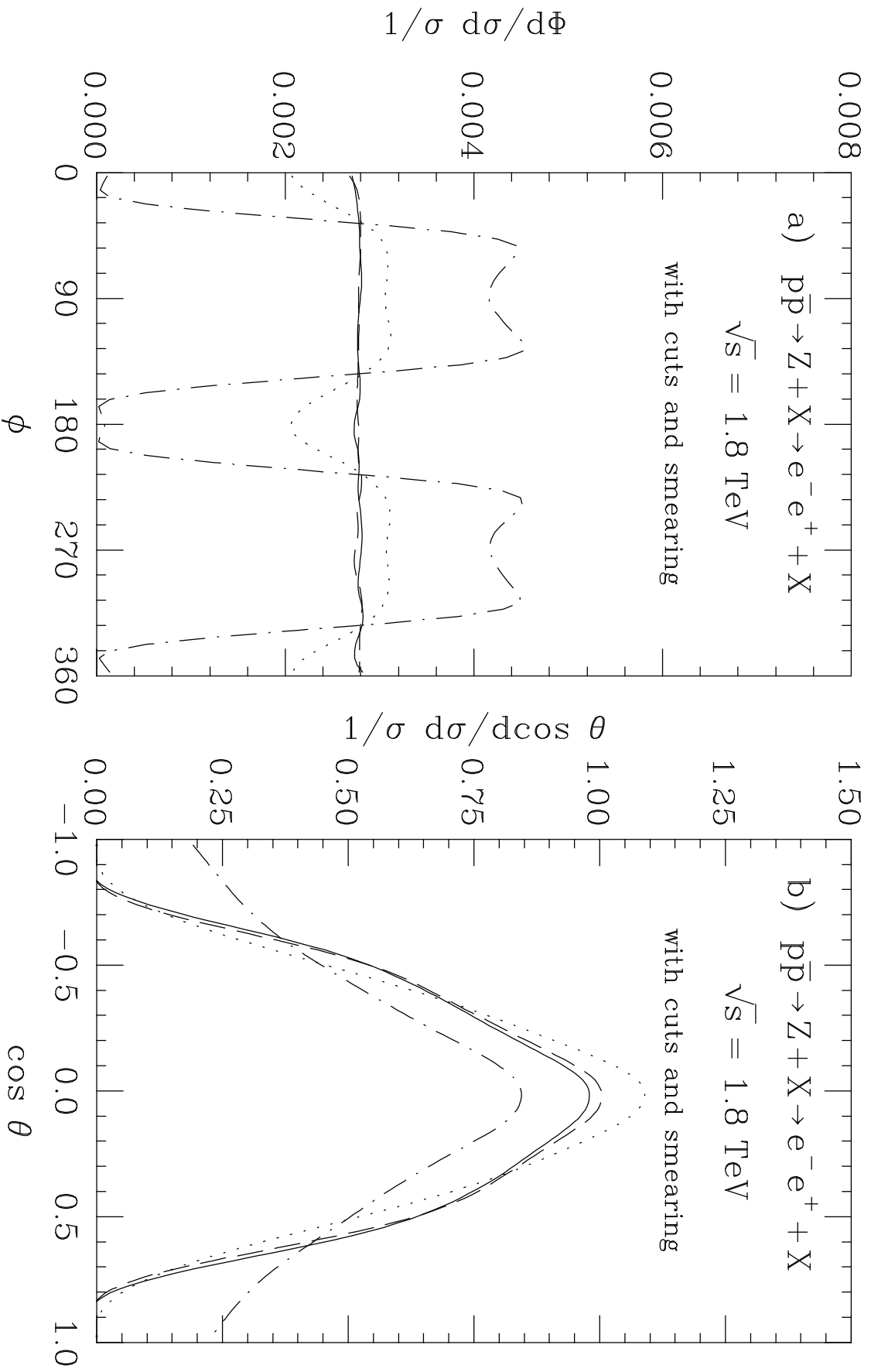


Figure 10

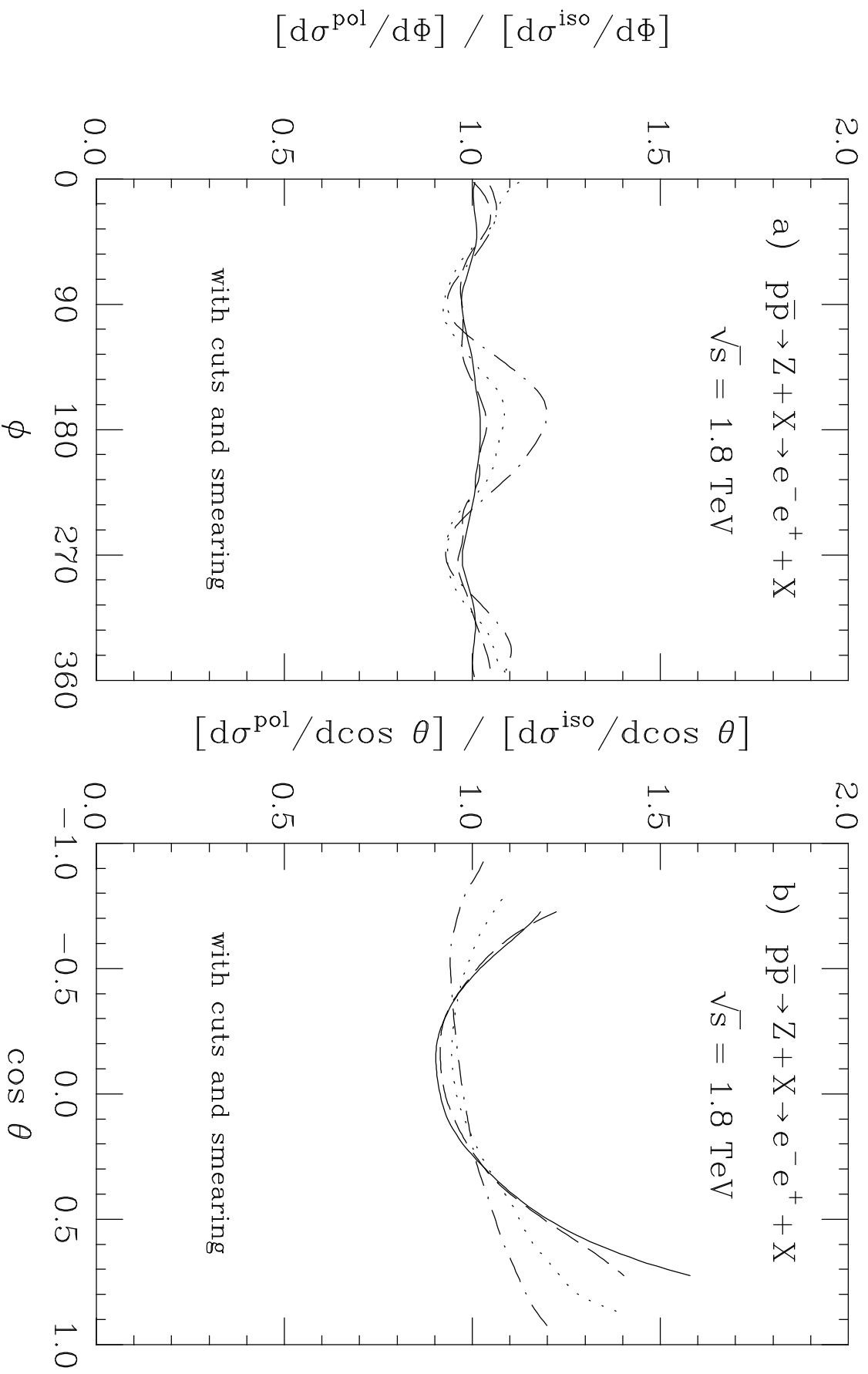


Figure 11

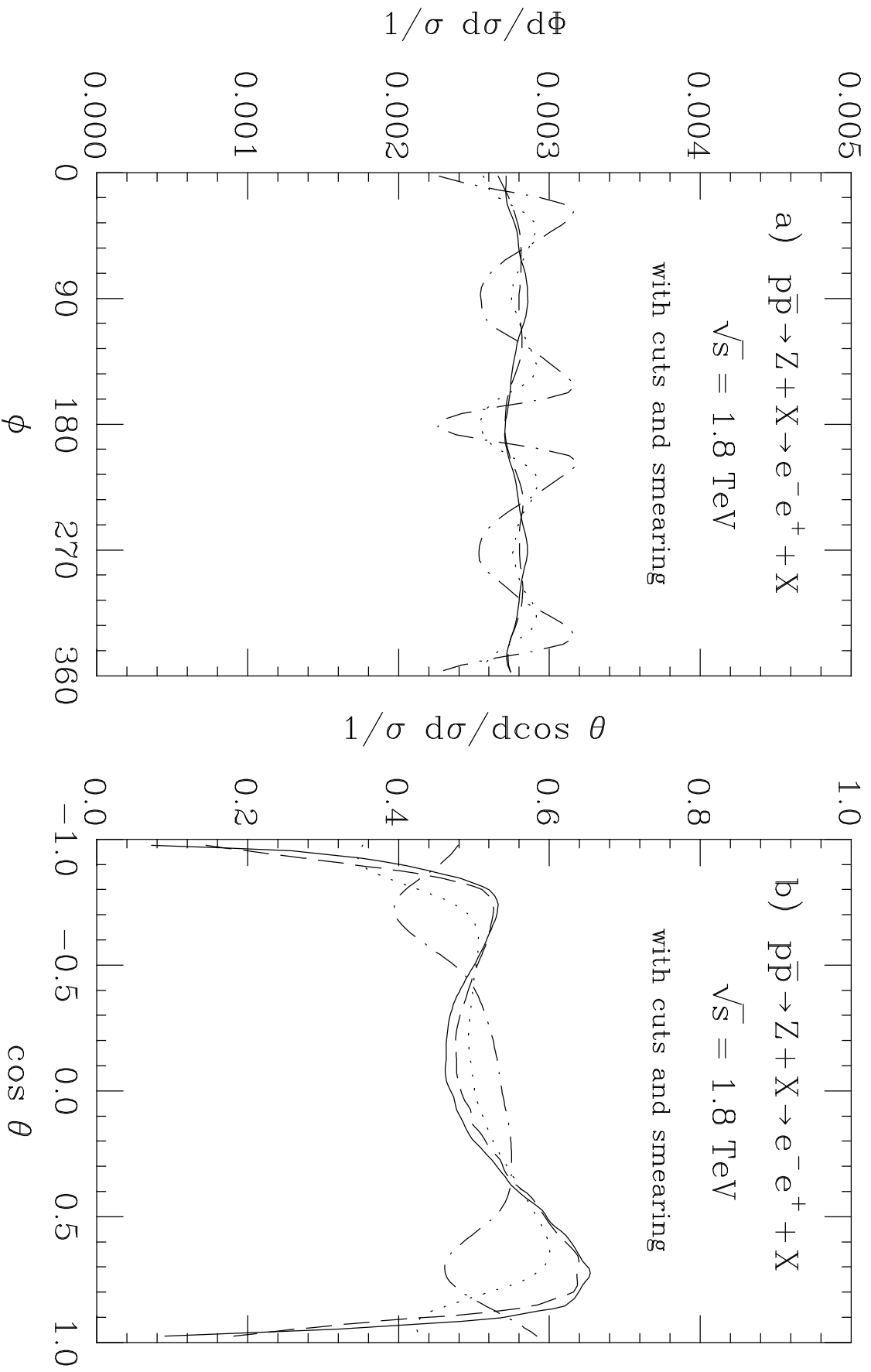


Figure 12

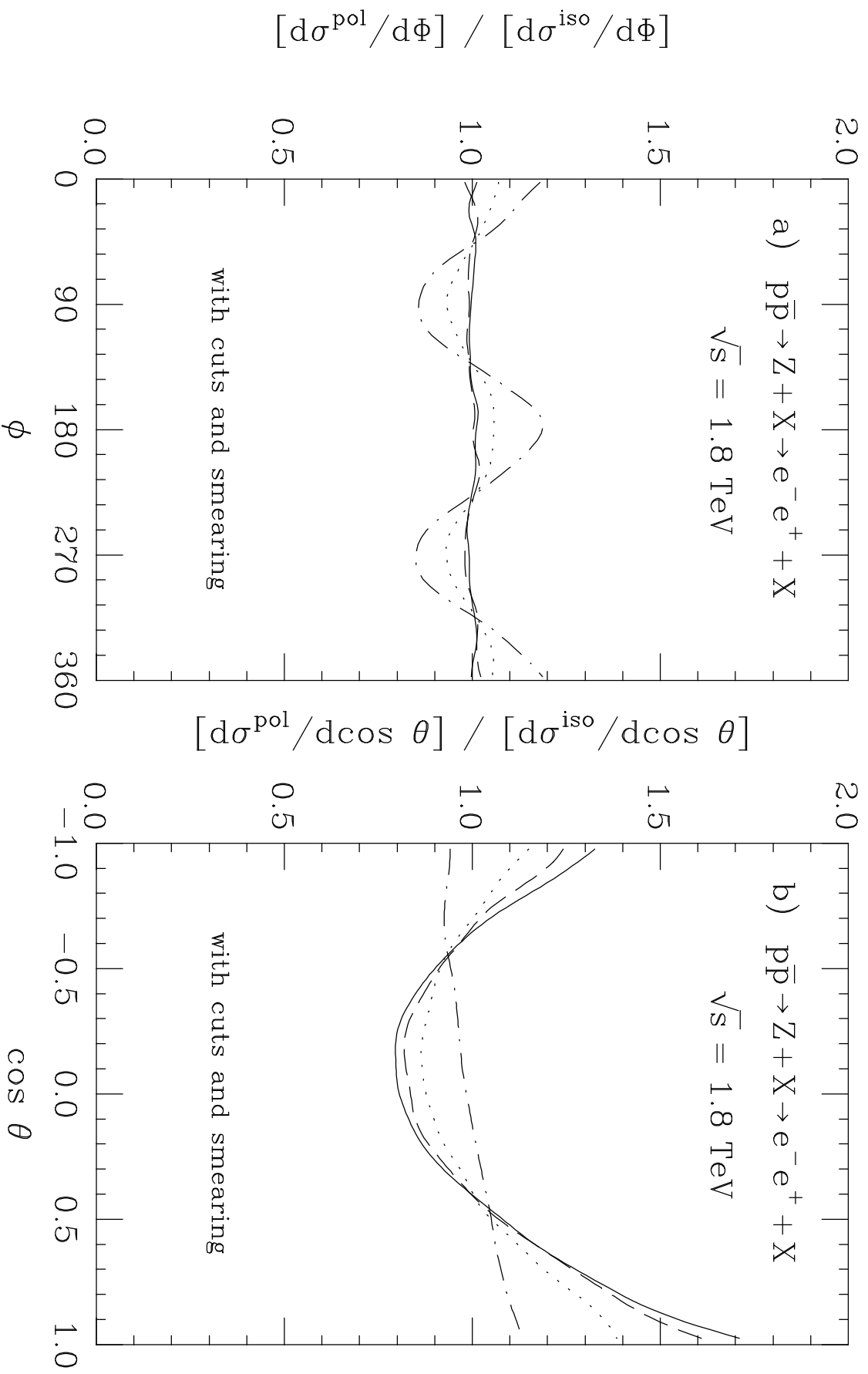


Figure 13